Structures 57 (2023) 105298

Contents lists available at ScienceDirect

Structures

journal homepage: www.elsevier.com/locate/structures

Investigation of the performance of the self-centering steel plate shear wall considering stress relaxation in pre-stressed cables

Mahtabsadat Razavi [a], Nader Fanaie [b,*]

[a] Graduated M.Sc Student of Structural Engineering, Department of Civil Engineering, K. N. Toosi University of Technology, Tehran, Iran
[b] Associate professor, Department of Civil Engineering, K. N. Toosi University of Technology, Tehran, Iran

ARTICLE INFO

Keywords:
Self-centering connection
Self-centering steel plate shear wall
Relaxation phenomenon
Low-yield-point steel
Pre-stressed cables

ABSTRACT

Self-centring systems are one of the novel earthquake-resistant systems that can eliminate permanent earthquake-induced damage in buildings. In these systems, damage can be limited to those members that can be easily replaced after earthquakes. Self-centring steel plate shear walls (SC-SPSW) with pre-stressed cables combine the lateral load-resisting capacity of conventional SPSWs with the self-centring capabilities of PT beam-to-column connections and provide sufficient ductility and stiffness for the system. The stress relaxation phenomenon in pre-stressed cables can lead to stress reduction in cables with the passage of time. This phenomenon should not be neglected. In this study, the self-centering steel plate shear wall is simulated using finite element (FE) modeling and verified based on available experimental results; then, the effect of stress relaxation on stiffness and energy dissipation capability of the system is evaluated at different initial pre-stressing forces and time intervals. According to the results, after five years and for cables with a pre-stressing ratio of 0.7, the stiffness and dissipated energy have reduced by 26 and 5 percent, respectively, in comparison to the time just after pre-stressing. These values was 40 % and 2 % for stiffness reduction and energy dissipation capacity reduction, respectively when the cables were pre-stressed with the pre-stressing ratio of 0.9. Furthermore, A method is also suggested to improve the seismic performance of the self-centering connections which includes employing low yield point steel in energy dissipater devices. Results showed that the energy dissipation capacity of the system doubles by using low-point steel for the web plates. The cumulative dissipated energy was about 1.044 MJ with A1008 steel and it was increased to 2.058 MJ with LYP100 material. This increase was mostly observed after the 10th cycle of the hysteresis curve.

1. Introduction

During the 1994 Northridge earthquake and the 1995 Kobe earthquake, the welded moment frames used as earthquake-resistant systems in these areas suffered the brittle failure of their beam-column connections [1]. After this incident, researchers conducted research to improve the seismic performance of moment frames. This included beam-column connections with reduced flanges and connections strengthened with cover plates and side plates.

To avoid damage in the form of yielding and local buckling of the main structural members leading to their permanent deformation, buildings can be designed to limit damage to those members that can be easily repaired or replaced. The structural system with this capability is called a self-centring system.

Self-centring connections in steel frames and steel plate shear walls are designed to eliminate inelastic deformation and residual lateral displacement in structural members due to earthquakes. This deformable behaviour is produced by creating a gap at the post-tensioned connection. The deformation capacity of this system against lateral forces is very high, and unlike steel frames that rely on the ductility and toughness of structural members, the behaviour of self-centring structures is not controlled by the deformation capacity of the materials. The energy loss during seismic loading is not due to the failure of the main structural members but to elements designed as energy dissipaters that can be replaced in case of failure.

Much research has been done to investigate the behaviour of self-centring connections in steel frames. Movaghati et al. propose a new post-tensioning configuration for improving the seismic performance of existing steel bolted connections [2]. Through experiments and analysis, the proposed connection was found to have increased stiffness, strength,

* Corresponding author at: University of Technology, Civil Engineering Department, No. 1346, Vali-Asr Street, P.O. Box. 15875-4416, 19697 Tehran, Iran.
E-mail address: fanaie@kntu.ac.ir (N. Fanaie).

https://doi.org/10.1016/j.istruc.2023.105298
Received 31 July 2023; Received in revised form 7 September 2023; Accepted 23 September 2023
Available online 2 October 2023

and self-centring capabilities. In addition, an analytical equation was derived to accurately represent the moment-rotation relationship and can be used to design and analyze post-tensioned connections under large deformations.

Cai et al. present a self-centring post-tensioned precast beam-to-column connection for earthquake-resistant structures [3]. Cyclic loading tests and numerical simulations show it has large initial stiffness, good re-centering capacity, and high ductility with deformation concentrated in easily replaceable steel angles. Appropriate PT strand areas, initial pre-stress, and concrete compressive strength improve its load-carrying and deformation capacities, while increasing beam cross-sectional width may improve its ductility.

Saeizadeh et al. propose a self-centring beam-column connection with friction dampers to address issues in conventional steel connections [4]. Experimental and finite element analyses were performed to study the effects of post-tensioning and pin pre-tensioning forces, strand diameter, and strand spacing on the connection's performance. The proposed connection showed stable behaviour up to a drift of 7 % without residual rotation and had lower installation costs.

Fanaie et al. investigated the behavior of self-centering steel plate shear wall in fire loading [5]. Based on the results, using fire-resistant coating for the steel members can improve the post-fire seismic performance of SC-SPSW system.

2. Overview of the behavior of PT connection

The anticipated hysteresis pattern of a post-tensioned energy dissipator (PTED) connection for a beam-column is expected to be in the shape of a flag. This behaviour is defined by its non-linear characteristics, ability to self-center, and capacity to dissipate energy. Fig. 1 illustrates the hysteresis pattern of a PTED connection.

In PTED connections, a post-tensioned member is used to transfer internal forces, which creates an even distribution of compression contact stresses at the intersection of the beam and column. Friction between the beam and column allows the transmission of shear force. Once the PT force is applied, the connection behaves rigidly, transmitting bending moments and shear forces without any relative rotations between the beam and column for small values of bending moments. However, for larger bending moments, a gap is formed at the beam-to-column interface, which leads to the elongation of the PT element in the elastic field, and the connection tends to return to its initial configuration. During this process, the energy dissipator devices deform due to relative movement between the beams and columns, and the input energy is dissipated in a stable manner, which confines damage to the energy dissipator devices. Fig. 2 displays the assembly and free-body diagram of the PTED beam-to-column connection.

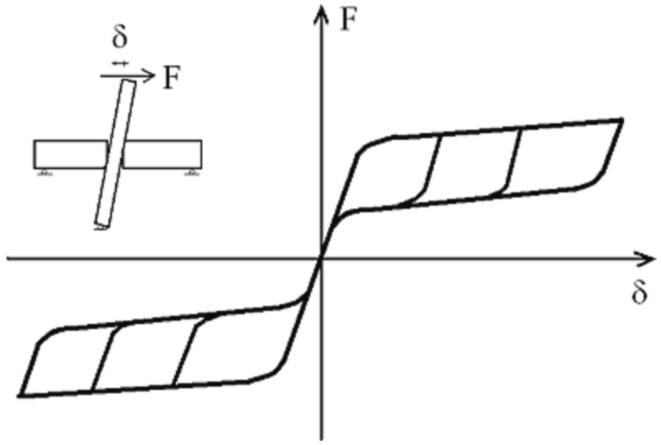

Fig. 1. Flag shaped hysteresis behavior of a PTED connection [6].

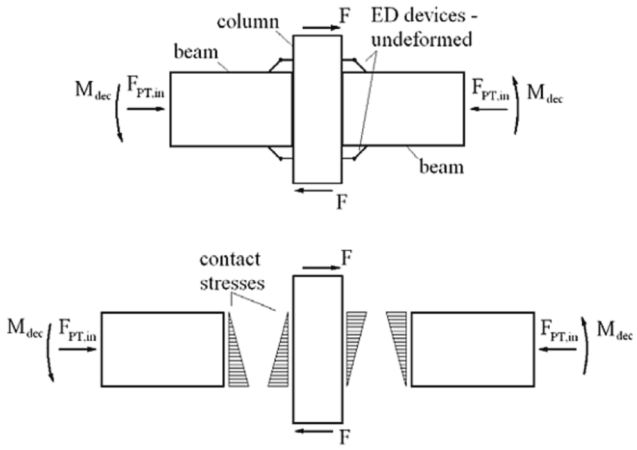

Fig. 2. Assembly and free body of PTED beam-to-column connection [6].

3. Self-centering steel plate shear wall system

The self-centring steel plate shear wall system is a new lateral load-resisting system that combines the strength and stiffness properties of the shear wall with the self-centring property of the post-tensioned beam-column connection.

The properties of the SPSW system can be improved by combining it with the self-centring capability based on pre-tensioned steel cables to restore the structure to its original condition after an earthquake. This is achieved through the use of yielding steel elements, which are designed to dissipate energy and maintain the integrity of the structure during and after an earthquake. The innovative design of SC-SPSWs enables the system to effectively resist lateral loads while maintaining excellent structural performance, making it an attractive option for seismic-resistant construction. Fig. 3 shows an SPSW system with self-centring capability consisting of web plates, post-tensioned connections, horizontal boundary elements (HBE), and vertical boundary elements (VBE) [7]. The difference between the presented models for self-centring shear walls lies in the elements that dissipate energy and the elements that enable the self-centring capability.

Clayton et al. presented a design method based on seismic

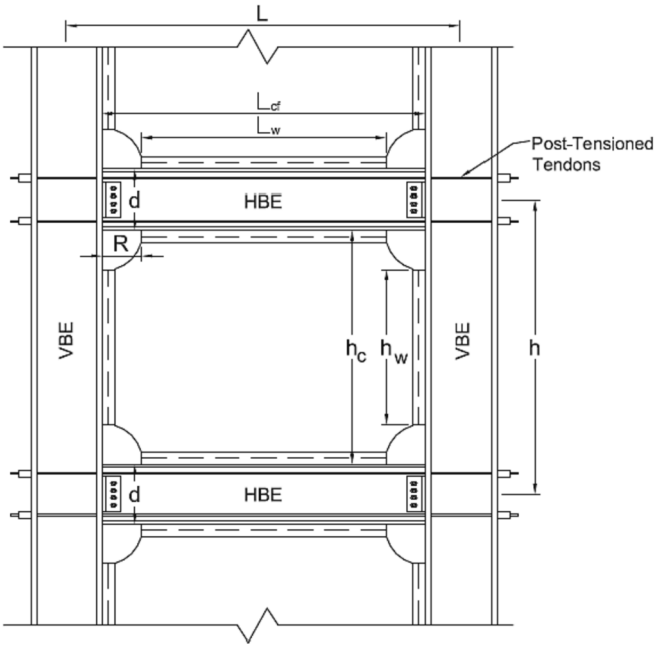

Fig. 3. Configuration of the SC-SPSW system [7].

performance levels for self-centring steel plate shear wall systems using time history analysis [8]. In this system, the web plates are considered as energy dissipating elements and enter the plastic region, while the beams and columns remain elastic. Clayton combines the lateral load-resisting capacity of conventional SPSWs with the self-centring capabilities of PT beam-to-column connections. The results of the non-linear dynamic response history analysis were used for the investigation of the SC-SPSW behaviour and design procedure.

The ideal hysteresis curve of all SC-SPSW systems is flag-shaped. This ideal curve can be seen in Fig. 4(a). In these systems, as mentioned earlier, most of the system resistance and energy dissipation is provided by the steel plate shear wall, and the pre-stressed connections give the system the self-centring capability. When a lateral load is applied, the SC-SPSW system has an initial stiffness, *Ki*. This stiffness is equal to the initial stiffness of the conventional shear wall system. After the connection enters the limit state of no compression (limit state 1 in Fig. 4 (a), the steel plate shear wall resists the lateral load by creating a tension field until the plate eventually yields (limit state 2 in Fig. 4(a)). After this limit state, as seen in the figure, the lateral stiffness of the structure decreases significantly. During loading (limit state 3 in Fig. 4(a)), the elastic stiffness of the plate is restored. After full unloading (limit state 4 in Fig. 4(a)), the pre-stressed connections are compressed again and cause self-centring stiffness, Kr, and bring the displacement in the structure to zero (limit state 5 in Fig. 4(b)) [8].

Although self-centring systems have shown better behaviour than semi-rigid connections in many studies, there are no appropriate guidelines for the design of these systems. Therefore, finite element modelling is a suitable method to analyze the behaviour of self-centring systems. To date, many finite element studies have been conducted to determine the effects of various factors on the behaviour of self-centring systems. In this study, the finite element model of the 2-story SC-SPSW is developed on Abaqus software verified with the experimental results from Clayton et al. [9]. The stress relaxation phenomenon in PT strands was then investigated, and the effect of plate material was evaluated through cyclic analysis on the FE model.

4. Modelling approach

The Abaqus software was used to create a numerical model of the 2-story SC-SPSW system investigated experimentally by Clayton et al. [9]. The system fails due to the buckling of web plates, so accurately modelling web plate response is crucial. Previous studies suggest that the Abaqus model is better at representing web plate response compared to other finite element software. Additionally, only the Abaqus model is capable of investigating the impact of various design parameters, such as web plate thickness and post-tension force, on seismic demand parameters to understand their effect on SC-SPSW behaviour. The modelling phases for Abaqus and their details are explained below.

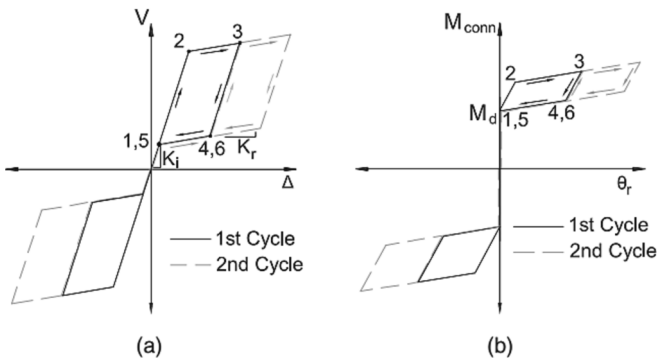

Fig. 4. Idealized SC-SPSW (a) system and (b) PT connection response [8].

4.1. Material properties and layout

In this study, the self-centering steel plate shear wall system experimentally investigated by Clayton et al. was selected and its 3D finite element model was developed using Abaqus software. The experimental setup of the model is shown in Fig. 5.

The two-story shear wall model includes three horizontal boundary elements (HBE) with a cross-section of W14 × 90, two vertical boundary elements (VBE) with a cross-section of W14 × 132, pre-stressed cables, and steel web plates. Eight pre-stressed cables are used on each floor. The center distances of the columns and beams are 3235 and 1724 mm, respectively. As mentioned earlier, beams and columns in this system remain elastic, and no plastic joint is formed in them, so a Wire element was used for their modelling.

Since the connections are rocking and not rigid, the depth of the beam and column must be introduced to the software. The rigid offset element was used to model the beam and column depth. The pre-stressed cables are braced at the outer edge of the column to create a rocking connection. Since the steel plates play the role of energy dissipaters of the system, the shell element was used to model them. The steel plates are located directly under the beam flanges and have dimensions 1367 × 2117 with a thickness of 1.5 mm per floor.

To create initial defects in steel plates, a small out-of-plane deformation is created by buckling analysis and the results are used in the model analysis.

The members of the steel frame, including the beams and columns, are made of A992 steel. The steel plates are ASTM A1008 and the pre-stressed cables are ASTM A416. The specifications of the materials used in the model are listed in Table 1.

4.2. Modeling of the connections

The interaction between the steel plates and the frame members is modelled using the tie constraint. In this case, no relative motion between two members is possible. Considering that the welded components are not damaged during the test, using the tie constraint instead of modelling the welds does not affect the result of the analysis. The tie constraint is also used to simulate the connection of the cable end to the end edge of the column.

Since the beam-column connection itself is a simple connection with a single web angle bar, and there are pre-stressed cables that provide rigidity in this connection, we use the coupling constraint to simulate the beam-column connection. In this case, only gravity loads are

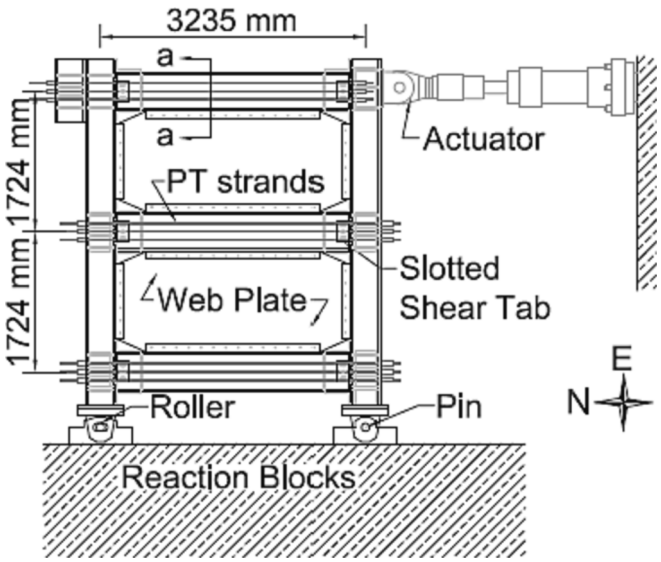

Fig. 5. SC-SPSW subassembly setup [9].

Table 1
Material properties of the FE model.

Ultimate Stress (MPa)	Yield Stress (MPa)	Poisson's Ratio	Modulus of Elasticity (MPa)	Material	Element
496	345	0.3	2×10^5	ASTM A992	Beam
496	345	0.3	2×10^5	ASTM A992	Column
1900	1620	0.3	1.96×10^5	ASTM A416	Cables
430	180	0.3	2×10^5	ASTM A1008	Steel panels

transferred, and the connection is simulated as a simple connection.

The simulation of the rocking operation of the connection is done by creating a gap in the connection. When the lateral force is applied to the frame from right to left, the upper right edge of the beam and the lower and left flanges of the beam transmit the force, while there is a gap at the other two corners, and there is no force transmission. Therefore, the simulation of the force transmission process should be done in such a way that the force is transmitted in compression and act neutral in tension, i.e. the gap at these points should be implemented only as a compression spring, and the axial force transmission is done by these springs. The simulation of these springs is done with the create connection section tool, and only the axial force is introduced in the force transmission section. Since these springs work only under compression, we set their specifications so that their tensile strength is negligible compared to the compressive strength. After setting the spring specifications, we placed these springs in the gaps we had already created in the model. Namely, these springs are placed at the connection between the top and bottom edges of the beam and the column. During loading, a force is applied to one of these edges (compression edge), and the other edge (tension edge) does not transmit any force. Details on connection modeling in Abaqus is shown in Fig. 6.

4.3. Loading and boundary condition

Hinged boundary conditions are considered for the bottom of the two columns. In this case, movement in all directions is not allowed, but it is allowed to rotate freely. The tie constraint of the rigid object was used to assign the above support conditions. The pre-stressing force of the cables was simulated by reducing the temperature and thermal load in the

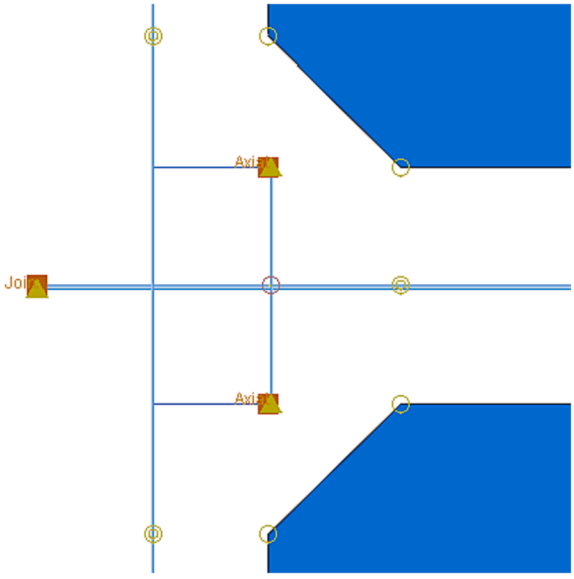

Fig. 6. Details of PT beam-column connection in Abaqus.

model. The method for calculating the temperature reduction to generate the pre-stressing force is as follows.

$$\frac{PL}{AE} + \alpha L \Delta T = 0 \tag{1}$$

where P is the pre-stressing force, L and A are the length and area of cables, E is the modulus of Elasticity of cables, and ΔT is the temperature change. According to the above-mentioned data, the pre-stressing force is 334 kN and the number of cables is 8. Considering $\alpha = 12 \times 10^{-6}$ and the total area of the cables is 1061 mm^2, and using Eq. (1), the amount of temperature change to generate the pre-stressing force is calculated to be 133 °C.

Considering the loss of pre-stressing force due to the shortening of the beam, we should calculate the amount of this loss and reduce the temperature a little more to compensate for the loss of force. For pre-stressed elements we have:

$$T_s = T_0 + \Delta T \tag{2}$$

where T_0 is the initial pre-stressing force applied when the system was built, and ΔT is the loss of pre-stressing force of the cable.

The loss of pre-stressing force is caused by the shortening of the HBE under the axial compressive force of the column and the axial compressive force caused by the elongation (increase in length) of the pre-stressed elements at the time of connection opening [7]. The amount of axial shortening of the beam is calculated as follows:

$$\Delta_{loss} = \frac{P_{PT} L_{HBE}}{A_{HBE} E_{HBE}} + \frac{P_{HBE(VBE)} L_{HBE}}{A_{HBE} E_{HBE}} = \frac{P_{PT}}{k_{HBE}} + \frac{P_{HBE(VBE)}}{k_{HBE}} \tag{3}$$

where P_{PT} represents the axial compressive force on the HBE from the prestressed elements and $P_{HBE(VBE)}$ is the axial compressive force on the HBE from the column. By solving Eq. (3), we obtain:

$$P_{PT} = k_{HBE} \Delta_{loss} - P_{HBE(VBE)} \tag{4}$$

Based on this equation, the effective net tensile force in the pre-stressed element is:

$$T_{PT} = k_{PT} (\Delta_{drift} - \Delta_{loss}) \tag{5}$$

In the above equation, Δ_{drift}, which is associated with the elongation of the cables and the connection opening, equals to:

$$\Delta_{drift} = \varnothing_{drift} d \tag{6}$$

where $\varnothing_{drift}$ represents the relative angle between HBE and VBE and d represents the beam depth. Since $T_{PT} = P_{PT}$, the value of Δ_{loss} is:

$$\Delta_{loss} = \frac{P_{HBE(VBE)}}{k_{HBE} + k_{PT}} + \left(\frac{k_{PT}}{k_{HBE} + k_{PT}}\right) \Delta_{drift} \tag{7}$$

Eventually, T_s that also includes losses caused by the beam shortening is equal to:

$$= T_0 + \frac{A_{PT} E_{PT}}{L_{PT}} \left(\Delta_{drift} - \Delta_{loss}\right) \tag{8}$$

Considering the above equations, a temperature reduction of 145 °C is suitable to produce the mentioned pre-stressing force.

In the experiment of Clayton et al. [9], the loads are applied to the top of the column by an actuator. The loading protocol is the same as in ATC-24 [10]. The history of the imposed cyclic lateral displacement based on ATC-24 is shown in Fig. 7. The finite element model was tested up to a lateral displacement of 4 %.

The applied loads include the initial failure load at the center of the plate as a concentrated load and a displacement-controlled loading at the top of the column.

The analysis is performed in three time steps. In the first step, the initial failure is generated by applying a concentrated load to the plate and buckling analysis. This step is necessary for considering the

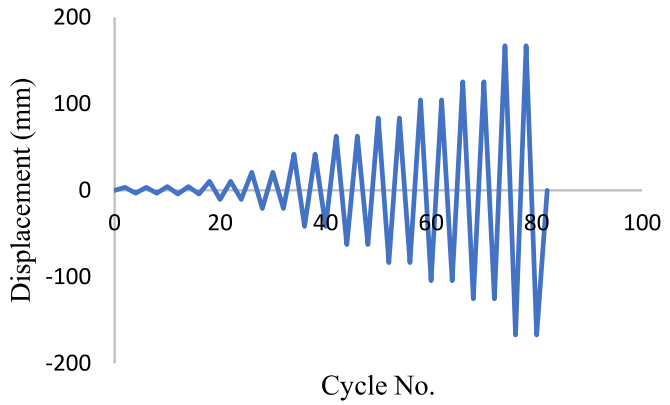

Fig. 7. The Cyclic loading protocol for the SC-SPSW, based on ATC-24.

imperfection of the web plates and the results of buckling analysis will be the primary condition for cyclic and push-over analysis. In the second step, the pre-stressing force is applied by applying the thermal load to the cables, and in the third step, the cyclic load is applied to the model in the form of displacement.

4.4. Meshing

As mentioned earlier, the web plates were simulated using S4R quadrilateral shell elements that have five Gauss integration points throughout the thickness. These elements are versatile and sturdy, making them suitable for various applications. They use a uniformly reduced integration technique to prevent shear and membrane locking, allowing them to model shell behaviour accurately. The B31 element was used for meshing the columns and beams, and the T3D2 element was used for meshing the prestressed cables. The sensitivity analysis of mesh size showed that the influence of mesh size on the results of this model is less than 5 %. The optimum mesh size for steel plates is 50 mm.

5. Model verification

The finite element model of the two-story steel shear wall system experimentally studied by Clayton et al. [9] was developed according to the previous section. Fig. 8 compares the lateral force–displacement response ratios obtained from the finite element analysis with the corresponding experimental response. The lateral force–displacement response ratios were measured at the loading point at the top of the column. It can be observed that the finite element modelling has sufficient accuracy and was able to predict the stiffness, yield strength, and strength of the specimen. The area under the hysteresis curves of the experimental and numerical models shows that the difference in the total energy dissipation for these two models is less than 10 %. Furthermore, the maximum stress in the frame members was 210 MPa based on the analysis results. According to the yield stress of frame members, which is 345 MPa, there are no regions of high stresses that lead to the plastic hinges in beams and columns.

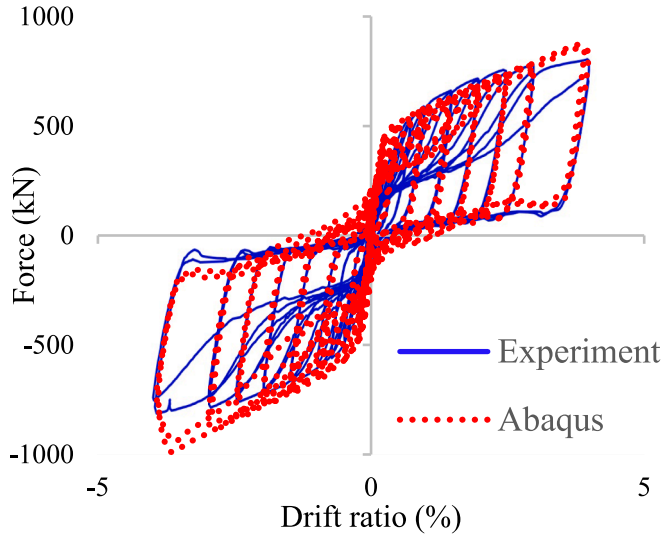

Fig. 8. Comparison of the hysteresis response of the experimental and Abaqus model.

6. Stress relaxation phenomenon

In general, the behaviour of the structure is a combination of its long-term and its instantaneous behaviour. Creep and stress relaxation phenomena are examples of the long-term behaviour of the structure. The literature recommends considering the effects of long-term phenomena on the performance of the structure. The stress relaxation phenomenon reduces the stress in pre-stressed steel. Ignoring this stress loss does not give a correct insight into the long-term behaviour of the structure. If this phenomenon is not taken into account when designing a structure, it can lead to incorrect design and cause significant damage to the structure. Fig. 9 shows the effect of stress relaxation on the pre-stressed cables. As it is shown in the figure, the structure exhibits an immediate reaction to the load within a brief period, t_0. The extended-term performance of the structure becomes apparent over a more extended duration, which varies depending on the materials and support conditions.

Empirical formulations are suggested in order to estimate the reduction of stress in a pre-stressed cable over time. Magura et al. estimated stress relaxation in pre-stressed members [12]. Experimental tests were performed under various conditions on pre-stressed cables, and an equation was established to predict the amount of stress relaxation. In this equation, stress relaxation depends on two factors: time and initial pre-stress ratio. Magura et al. established Eq. (9) to approximate the amount of stress relaxation:

$$\frac{f_s}{f_{si}} = 1 - \frac{logt}{10}\left(\frac{f_{si}}{f_y} - 0.55\right) for \frac{f_{si}}{f_y} > 0.55 \tag{9}$$

where fs represents the residual stress in the cable after a specific time, fsi represents the initial stress, fy represents the yield stress, and t represents the time in hours.

Research has been conducted to evaluate the effects of the stress relaxation phenomenon on the behaviour of structures. Zeren et al. studied the stress relaxation phenomenon in carbon cables with a

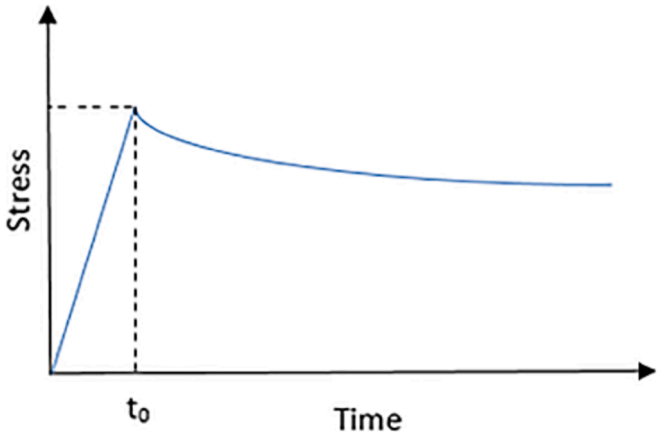

Fig. 9. The effect of stress relaxation on pre-stressed cables [11].

diameter of 8 mm [13]. By conducting empirical studies and considering experimental relationships, Zeren et al. concluded that the largest stress relaxation occurs at 400 °C. The stress relaxation increases with temperature. Moreover, stress relaxation increases with time and with the increase of the tension ratio of the cables. Zeren et al. established equations to estimate stress relaxation as a function of time and tension ratio.

Francis et al. investigated the effects of time-dependent phenomena in cable-stayed bridges [14]. In this study, after developing the finite element model of the cable-stayed bridge, linear non-geometric effects were applied, and dynamic analysis was performed over a long period. According to the results, the stress relaxation of the cables has less effect on the natural frequencies of the structure than the creep of the concrete.

Wang et al. investigated the stress relaxation phenomenon in certain types of structural cables [15]. Experimental studies were conducted on five types of cables with initial pre-stressing ratios of 70, 55, and 40 %. Also, three temperature conditions of 15, 20, and 25 °C were applied. The results showed that the relationship between time and stress relaxation of specimens is logarithmic. Moreover, the rate of stress relaxation increases with increasing temperature and increasing pre-stressing ratio.

Asadollahi and Fanaie studied the stress relaxation phenomenon in self-centering connections of steel moment frames [16]. In this study, a self-centering steel moment frame was modeled in Abaqus FEA software and the amount of stress in pre-stressed cables was determined after 1, 5, 10, and 20 years from the time of pre-stressing. Based on the results, equations were established to estimate the stiffness reduction and dissipated energy due to the stress relaxation phenomenon.

In this study, we use finite element modeling to investigate the effects of the stress relaxation phenomenon in pre-stressed cables on the behavior of the self-centering system. For this purpose, the stiffness and lateral load resistance of the system are investigated after 0, 5, 10, and 20 years of pre-stressing and under different pre-stressing ratios.

7. Modeling the stress relaxation phenomenon

To analyze the stiffness of the connection, a static load in the form of a displacement was applied to the end of the beam on the second floor instead of a cyclic load. The configuration of the finite element model is shown in Fig. 10. The analysis was performed in two time steps. In the first step, a pre-stress force is applied to the cables, and in the second step, a point load is applied to the end of the beam. The point load increases immediately after the pre-stressing is completed.

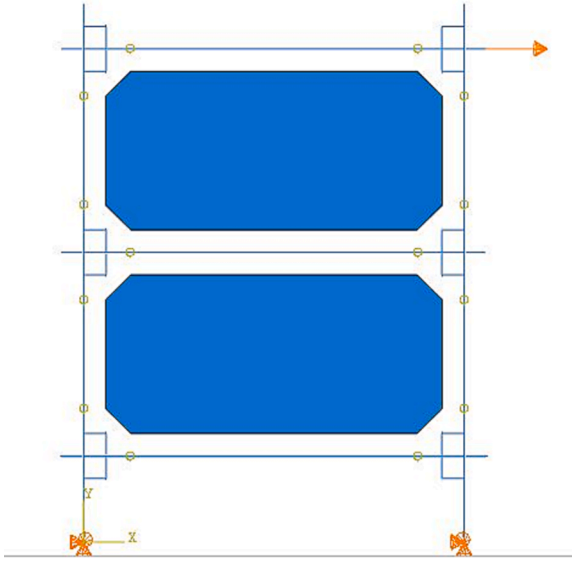

Fig. 10. SC-SPSW finite element model configuration.

The pushover diagrams of the system for pre-stressing ratios of 0.2, 0.5, 0.7, and 0.9 are shown in Fig. 11. These diagrams refer to the time immediately after the load is applied. As can be seen from the figure, the higher the pre-stressing ratio, the lower the deformation of the connection for the same force application.

Also, the values of the slope of the pushover diagram at the pre-stressing ratios of 0.2, 0.5, 0.7, and 0.9 are 1.006, 1.07, 1.086, and 1.089 kN/mm, respectively. The stiffness values refer to the load immediately after pre-stressing of the cables. As shown, the elastic deformation of the system is very small compared to the pre-stressing force.

Analysis of the stiffness of SC-SPSW at different times and ratios of pre-stressing to analyze the effects of the stress relaxation phenomenon on the stiffness of the system, the finite element model of the self-centring shear wall with a pre-stressing ratio of 0.6, 0.7, 0.8, and 0.9 at times immediately after the application of pre-stressing and 1, 5, 10, and 20 years after the application of pre-stressing load was evaluated by pushover analysis.

The connection stiffness at different pre-stressing ratios and times is given in Table 2. As can be seen, the stiffness reduction under stress relaxation is negligible at a pre-stressing ratio of 0.6, and as the pre-stressing ratio increases, the stiffness reduction increases with time. In addition, the largest stiffness reduction occurs in the first year after pre-stressing, and then the stiffness reduction decreases. Table 3 shows the ratio of the stiffness of the self-centring shear wall connection at different times compared to the initial stiffness of the connection.

Considering the fifth year as the basis of comparison, connection stiffness reduced by 9, 26, 36, and 40 % compared to the initial stiffness for pre-stressing ratios of 0.6, 0.7, 0.8, and 0.9, respectively. The ratio of connection stiffness at the indicated times to the initial stiffness is shown in Table 3 and on the vertical axis of Fig. 12. Based on the diagram and the obtained data, the following equation can be established to estimate the amount of stiffness reduction:

$$\frac{K_t}{K_0} = 1 - 1.8\frac{logt}{10}\left(\frac{f_{si}}{f_y} - 0.55\right) \tag{10}$$

where K_0 is the initial stiffness of the connection, t is the time in seconds, K_t is the connection stiffness at time t after pre-stressing, and f_{si}/f_y is the ratio of initial stress to yield stress.

8. Analysis of the effects of the stress relaxation on the energy dissipation of the SC-SPSW

To analyze the load–displacement diagram under cyclic loading and consider the stress relaxation phenomenon, the finite element model of the self-centering shear wall system was developed according to the experimental model. This time, a displacement-controlled cyclic load was applied to the endpoint of the beam on the second floor.

To investigate the cyclic behavior of the connection under the stress

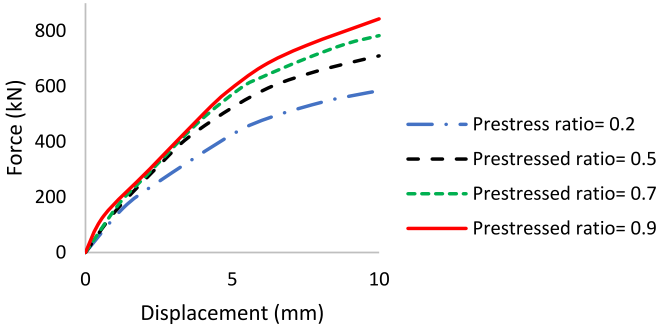

Fig. 11. Push over curves of SC-SPSW system at different pre-stressing ratios.

Table 2
Stiffness of the SC-SPSW system at different times and pre-stressing ratios (kN/mm).

Fs/*FsiT* (year)	0.6	0.7	0.8	0.9
0	15.6	20.77	23.88	24.52
1	14.5	15.7	15.66	15.05
5	14.2	15.46	15.3	14.61
10	14.2	15.02	14.94	13.87
20	14.2	14.8	14.71	12.97

Table 3
The ratio of the stiffness of the self-centering shear wall connection (F_s) at different times, to the initial stiffness of the connection (F_{si}).

Fs/*FsiT*(year)	0.6	0.7	0.8	0.9
0	1	1	1	1
1	0.93	0.76	0.66	0.61
5	0.91	0.74	0.64	0.6
10	0.91	0.72	0.63	0.57
20	0.91	0.71	0.62	0.53

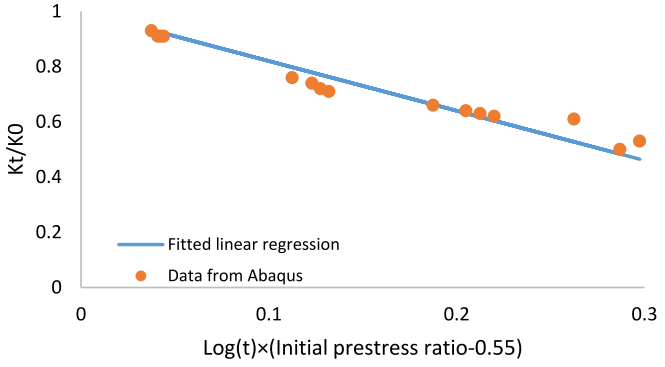

Fig. 12. Estimation of stiffness reduction in SC-SPSW due to stress relaxation.

relaxation phenomenon, the energy dissipation was calculated by calculating the area inside the force–displacement hysteresis curve for the different pre-stressing ratios and times. The results of the hysteresis analysis with pre-stressing ratios of 0.6, 0.7, 0.8, and 0.9 at 1, 5, 10, and 20 years after the pre-stressing are shown in Table 4. Table 4 shows that the stress relaxation phenomenon reduces the energy dissipation of the system over time and that the amount of energy reduction increases with the increase of the pre-stressing ratio. When the pre-stressing ratio is 0.6, the effect on the connection behavior over time is insignificant, and when the initial pre-stressing ratio is increased, the reduction in energy dissipation over time becomes significant. The energy dissipation of the system in the indicated times compared to the initial energy dissipation is shown in Table 5 and on the vertical axis of Fig. 13. Using the diagram, Eq. (11) can be established to estimate the reduction of energy dissipation of the system.

Table 4
Cumulative dissipated energy of the SC-SPSW system at different times and pre-stressing ratios (MJ).

Fs/*FsiT*(year)	0.6	0.7	0.8	0.9
0	65.4	60.22	59.34	56.29
1	60.21	57.6	58.22	55.64
5	58.96	56.9	56.24	55.22
10	57.05	56.15	55.7	54.26
20	56.84	55.01	55.04	54.03

Table 5
The ratio of the cumulative dissipated energy of the self-centering shear wall connection at different times, to the initial energy dissipation capacity of the connection.

Fs/*FsiT*(year)	0.6	0.7	0.8	0.9
0	1	1	1	1
1	0.92	0.96	0.98	0.99
5	0.9	0.94	0.95	0.98
10	0.87	0.93	0.94	0.96
20	0.87	0.91	0.93	0.96

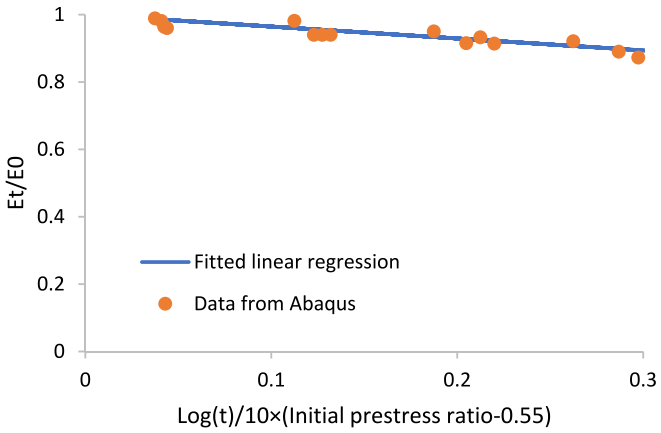

Fig. 13. Estimation of energy dissipation reduction in SC-SPSW due to stress relaxation.

$$\frac{E_t}{E_0} = 1 - 0.35\,\frac{logt}{10}\left(\frac{f_{si}}{f_y} - 0.55\right) \tag{11}$$

where E_0 is the initial energy dissipation, t is the time in seconds, E_t is the energy dissipation at time t after pre-stressing, and f_{si}/f_y is the ratio of initial stress to yield stress of the cable.

Considering the fifth year as the basis of comparison, the energy dissipation of the system reduced by 2, 5, 6, and 10 % compared to the initial stiffness when the pre-stressing ratio was 0.6, 0.7, 0.8, and 0.9, respectively.

9. The use of mild steel in web plates

Mild steel is a type of steel first developed in Japan for use in energy dissipation devices [17]. When a structure is subjected to seismic loading, the damage can be reduced by using advanced materials in structural members designed for energy dissipation. These structural members are capable of yielding before the other structural members and thus dissipate the earthquake energy by forming plastic joints [18]. Due to its low yield strength, moderate ductility, and low cycle fatigue performance, mild steel is a good alternative for the above-mentioned materials [19]. Many experimental and numerical research has been conducted to support the idea of using LYP steel as the web plate material in steel plate shear walls. The cyclic behavior of LYP steel plate shear wall was investigated by Chen et al. The experimental and analytical results showed that the LYP steel shear wall is able to maintain stable up to 3–6 % of story drift angle and excellent deformation capacity was obtained from LYP steel models [20].

To investigate the effects of using mild steel on the behavior of self-centering connections, LYP100 was used to define the plate materials in modeling. The other elements are made of ASTM A992 (A992) structural steel. Fig. 14 compares the stress–strain curve of A572 and LYP100 steel. As can be seen, LYP100 has no pronounced yield strength and its yield strain is one-fourth that of A572. The tensile strength of LYP100 is fifty

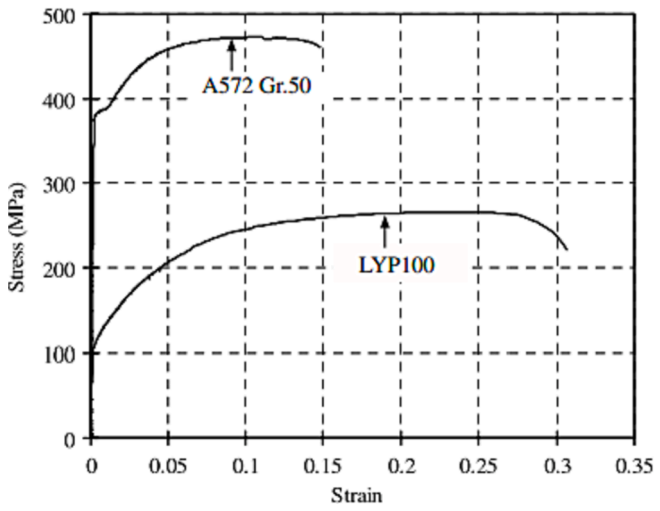

Fig. 14. Complete stress–strain curve for LYP and A572 structural steel [21].

percent higher than the tensile strength of A572 and also has a higher strain hardening in the plastic range. This steel grade has the same modulus of elasticity (E) as A572 structural steel and a low yield strength ratio ($\frac{F_y}{F_u} = 0.34$)), giving the structure a wider plastic zone [21].

Since the energy dissipating element in the self-centering steel plate shear wall system is the steel plate or web plates, the use of steel with lower yield strength in these elements can increase the deformation capacity and energy dissipation of the system. In the original model, ASTM A1008 steel with a modulus of elasticity of 213000 MPa and yield strength of 180 MPa was used for the plate. Here, these materials are replaced by LYP100 mild steel. The yield strength of this steel is 85 MPa and the ultimate strength is 275 MPa.

9.1. Calculation of the new dimensions of the steel plates

To analyze the effect of using mild steel in energy dissipation devices on the response of the self-centring connection, the dimension of the plate should be modified. The geometry of the plates was recalculated so that the element with the new dimensions could have the same yielding mechanism as the plate made of A1008 steel. The energy dissipation of the self-centring shear wall system is provided by the inelastic yielding of the web plates. When the system experiences lateral displacement, the steel web plate undergoes shear buckling, creating a tension field that counteracts the lateral forces. The shear strength of the web plates is calculated as follows.

$$V_n = 0.42 F_y t_w L_{cf} sin(2\alpha) \tag{12}$$

where F_y is the yield strength of the web plate, L_{cf} is the net distance between the VBE members, t_w is the thickness of the web plate, and α is the angle of tension field formation relative to the vertical direction, and is calculated using Eq. (13).

$$\alpha = arctan \sqrt{\frac{1 + \frac{t_w L}{2A_c}}{1 + t_w h\left(\frac{1}{A_b} + \frac{h^3}{360 I_c L}\right)}} \tag{13}$$

where t_w is the thickness of the web plate, h is the height of the floor, L is the length of the opening, I_c is the moment of inertia of the VBE, A_c is the cross-section of the VBE, and A_b is the cross-section of the HBE. As the lateral displacement increases, the web plate in the principal direction, which forms an angle α with the vertical direction, yields under stress and provides energy dissipation of the system.

Now, to produce a similar failure mechanism, the thickness of the steel plate with LYP materials is obtained by the equality of $V_{n(A1008)} = V_{n(LYP)}$. From the above equality, the thickness of the steel plate is 4.9 mm and modelling is done using this thickness in Abaqus software.

9.2. The consequences of using mild steel in steel plates

For better comparison, Fig. 15 also shows the diagram of equivalent dissipated energy as a function of the number of cycles of the hysteresis curve for the case in which the plates are made of LYP and A1008 steel. In this figure, the actual values of dissipated energy are normalized by the maximum dissipated energy. It can be seen that the capacity of energy dissipation increases when LYP steel is used.

After the analysis is completed, the total amount of dissipated energy is about 1 MJ when A1008 steel is used and about 2 MJ when LYP100 steel is used. As can be seen in Fig. 16, the energy dissipation capacity of the system is almost doubled when the steel used in the plate is replaced by mild steel.

10. Summary and conclusion

Self-centering systems are designed to reduce permanent damage to buildings during earthquakes, and one type of system is the self-centering steel plate shear wall with pre-stressed cables. This system combines the lateral load resistance of conventional walls with the self-centering abilities of beam-to-column connections. However, stress relaxation in the pre-stressed cables can reduce their effectiveness over time, which can affect the stiffness and energy dissipation capability of the system. This study evaluated the impact of stress relaxation on the system at different pre-stressing forces and time intervals. Finite element analysis were performed on models with pre-stressing ratios of 0.6, 0.7, 0.8, and 0.9 and stiffness and dissipated energy were recorded after 1, 5, 10, and 20 years after pre-stressing the cables. Based on analysis results, the ratio of the secondary stiffness to the initial stiffness of the connection is 0.76, 0.74, 0.72 and 0.71 after 1, 5, 10 and 20 years, respectively and at the pre-stressing ratio of 0.7. However, these ratios are 0.61, 0.6, 0.57 and 0.53 for the system with the pre-stressing ratio of 0.9. It was concluded that the stiffness reduction of the connection will increase by increasing the pre-stressing ratio of the cables.

To improve the cyclic performance of the self-centering connections, the use of low yield point steel in energy dissipater devices was suggested. LYP100 steel was used as the material for the steel web plates instead of A1008 which was used in previous analysis. The energy dissipation capacity of the system was evaluated when LYP material was assigned to the web plates. Results showed that the energy dissipation capacity of the system will be doubled by using LYP material. The total dissipated energy was recorded as 1.044 MJ with A1008 steel, while this value was increased to 2.058 MJ when LYP material was used. It was observed that in this case, the cumulative dissipated energy starts to

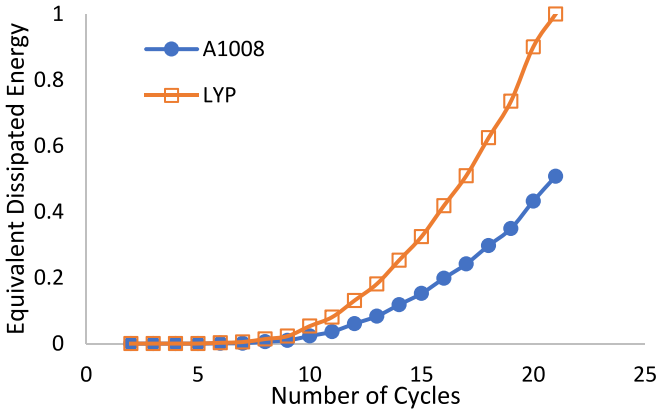

Fig. 15. Comparison of the cumulative equivalent dissipated energy in terms of number of cycles for LYP and A1008 steel.

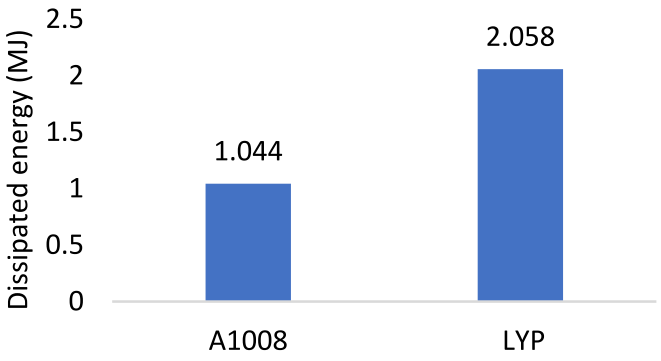

Fig. 16. Comparison of the total dissipated energy for LYP and A1008 steel.

increase after the 10th cycle of the hysteresis loading.

Declaration of Competing Interest

The authors declare that they have no known competing financial interests or personal relationships that could have appeared to influence the work reported in this paper.

References

[1] Engelhardt MD, Sabol TA. Reinforcing of steel moment connections with cover plates: benefits and limitations. Eng Struct 1998;20(4–6):510–20. https://doi.org/10.1016/S0141-0296(97)00038-2.
[2] Movaghati S, Abdelnaby AE. Experimental and analytical investigation of improved behavior of existing steel connections by adding self-centering capabilities. J Build Eng 2021;43:102543.
[3] Cai X, Pan Z, Zhu Y, Gong N, Wang Y. Experimental and numerical investigations of self-centering post-tensioned precast beam-to-column connections with steel top and seat angles. Eng Struct 2021;226:111397.
[4] Saeidzadeh M, Chenaghlou MR, Akbari Hamed A. Experimental and numerical study on the performance of a novel self-centering beam-column connection equipped with friction dampers. J Build Eng 2022;52:104338.
[5] N. Fanaie and M. Razavi, "Investigation of the performance of self-centering steel plate shear walls under fire loading," *Numer. Methods Civ. Eng.*, vol. 6, no. 4, pp. 67–77, 2022, 10.52547/nmce.6.4.67.
[6] M. Esposto, "PTED beam-to-column connections for steel moment resisting frames: structural identification based on numerical analyses," 2008.
[7] Dowden DM, Purba R, Bruneau M. Behavior of self-centering steel plate shear walls and design considerations. J Struct Eng 2012;138(1):11–21. https://doi.org/10.1061/(asce)st.1943-541x.0000424.
[8] P. M. Clayton, D. M. Dowden, T. Winkley, J. W. Berman, M. Bruneau, and L. N. Lowes, "Experimental investigation of self-centering steel plate shear walls," *Struct. Congr. 2012 - Proc. 2012 Struct. Congr.*, pp. 1586–1597, 2012, 10.1061/9780784412367.141.
[9] Clayton PM, Berman JW, Lowes LN. Subassembly testing and modeling of self-centering steel plate shear walls. Eng Struct 2013;56:1848–57. https://doi.org/10.1016/j.engstruct.2013.06.030.
[10] "ATC. Guidelines for seismic testing of components of steel structures. Tech. Rep. 24. Applied Technology," 1992.
[11] Saunders DW. Creep and relaxation of nonlinear viscoelastic materials. Polymer (Guildf) 1978;19(1):118. https://doi.org/10.1016/0032-3861(78)90187-8.
[12] Magura DD, Sozen MA, Siess CP. A study of stress relaxation in prestressing reinforcement. pcij 1964;9(2):13–57.
[13] Zeren A, Zeren M. Stress relaxation properties of prestressed steel wires. J Mater Process Technol 2003;141(1):86–92. https://doi.org/10.1016/S0924-0136(03)00131-6.
[14] Au FTK, Si XT. Time-dependent effects on dynamic properties of cable-stayed bridges. Struct Eng Mech 2012;41(1):139–55.
[15] Wang X, Chen Z, Liu H, Yu Y. Experimental study on stress relaxation properties of structural cables. Constr Build Mater 2018;175:777–89. https://doi.org/10.1016/j.conbuildmat.2018.04.224.
[16] Asadolahi SM, Fanaie N. Performance of self-centering steel moment frame considering stress relaxation in prestressed cables. Adv Struct Eng 2020;23(9):1813–22. https://doi.org/10.1177/1369433219900940.
[17] Saeki E, Sugisawa M, Yamaguchi T, Wada A. Mechanical properties of low yield point steels. J Mater Civ Eng 1998;10(3):143–52. https://doi.org/10.1061/(asce)0899-1561(1998)10:3(143).
[18] Wang J, Shi Y, Wang Y. Constitutive model of low-yield point steel and its application in numerical simulation of buckling-restrained braces. J Mater Civ Eng 2016;28(3):04015142. https://doi.org/10.1061/(asce)mt.1943-5533.0001416.
[19] Shih MH, Sung WP, Go CG. Investigation of newly developed added damping and stiffness device with low yield strength steel. J Zhejiang Univ Sci 2004;5(3):326–34. https://doi.org/10.1631/jzus.2004.0326.
[20] Chen SJ, Jhang C. Cyclic behavior of low yield point steel shear walls. Thin-Walled Struct 2006;44(7):730–8. https://doi.org/10.1016/j.tws.2006.08.002.
[21] Chen SJ, Jhang C. Experimental study of low-yield-point steel plate shear wall under in-plane load. J Constr Steel Res 2011;67(6):977–85. https://doi.org/10.1016/j.jcsr.2011.01.011.